METTL3-Mediated RNA m^{6}A Modification Regulates the Angiogenic Behaviors of Retinal Endothelial Cells by Methylating *MMP2* and *TIE2*

Yong Lin,[1] Guangying Luo,[1] Qi Liu,[1] Rusen Yang,[1] Peter Sol Reinach,[1] and Dongsheng Yan[1]

[1]State Key Laboratory of Ophthalmology, Optometry and Visual Science, Eye Hospital, Wenzhou Medical University, Wenzhou, China.

PURPOSE. N^6-methyladenosine (m^{6}A) is a commonly occurring modification of mRNAs, catalyzed by a complex containing methyltransferase like 3 (METTL3). Our research aims to explore how METTL3-dependent m^{6}A modification affects the functions of retinal endothelial cells (RECs).

METHODS. An oxygen-induced retinopathy (OIR) mouse model was established, and RECs were isolated using magnetic beads method. Human retinal microvascular endothelial cells (HRMECs) were treated with normoxia (21% O_2) or hypoxia (1% O_2). Dot blot assay determined m^{6}A modification levels. Quantitative RT-PCR and Western blot detected the mRNA and protein expression levels of the target candidates, respectively. Genes were knocked down by small interfering RNA transfection. Matrigel-based angiogenesis and transwell assays evaluated the abilities of endothelial tube formation and migration, respectively. Methylated RNA immunoprecipitation–qPCR determined the levels of m^{6}A modification in the target genes.

RESULTS. The m^{6}A modification levels were significantly upregulated in the retinas and RECs of OIR mice. Exposure to hypoxia significantly elevated both METTL3 expression and m^{6}A modification levels in HRMECs. METTL3 knockdown curtailed endothelial tube formation and migration in vitro under both normoxic and hypoxic conditions. Concurrently, this knockdown in HRMECs resulted in reduced m^{6}A modification levels of *MMP2* and *TIE2* transcripts, subsequently leading to a decrease in their respective protein expressions. Notably, knockdown of MMP2 and TIE2 also markedly inhibited the angiogenic activities of HRMECs.

CONCLUSIONS. METTL3-mediated m^{6}A modification promotes the angiogenic behaviors of RECs by targeting *MMP2* and *TIE2*, suggesting its significance in retinal angiogenesis and METTL3 as a potential therapeutic target.

Keywords: METTL3, m^{6}A, retinal angiogenesis, *MMP2*, *TIE2*

Retinal neovascularization is a hallmark of several eye diseases, including retinopathy of prematurity, diabetic retinopathy, and retinal vein occlusion,[1] which may ultimately lead to macular edema.[2] This aberrant response can cause vision loss and even result in irreversible blindness. The underlying cause of this abnormal response is ischemic hypoxia in the retina, which leads to a proteolytic breakdown of the basement membrane supporting the endothelial cells (ECs). The loss of support triggers increased migration and proliferation of ECs, leading to the growth of new blood vessels (angiogenesis).[3] Despite a growing number of studies investigating the molecular mechanisms behind these events, the challenge of effectively inhibiting retinal neovascularization in clinical settings remains unmet.

Retinal ischemia and hypoxia can induce neovascularization accompanied by upregulation of multiple angiogenesis-related factors, including vascular endothelial growth factor, erythropoietin, and angiopoietins (Ang-1 and Ang-2), and more.[1] In addition, epigenetic mechanisms, including DNA methylation,[4] histone modifications,[5] and noncoding RNAs,[6] are increasingly recognized as critical regulators of retinal EC (REC) proliferation, migration, and angiogenesis. RNA N^6-methyladenosine (m^{6}A) is the most widely occurring and reversible epigenetic modification of mRNAs in mammalian cells, characterized by a methylation at the N^6 position of adenosine.[7] It has been shown that m^{6}A modification regulates multiple biological processes by affecting RNA stability, mRNA degradation, and translation.[8,9] The m^{6}A modification status is controlled by methyltransferase complexes known as "m^{6}A writers," including methyltransferase-like 3 (METTL3), methyltransferase-like 14 (METTL14), Wilms tumor 1 associated protein (WTAP), as well as newly discovered m^{6}A writers, involving Vir-like m^{6}A methyltransferase associated,[10] zinc finger CCCH-type containing 13 (ZC3H13),[11] and RNA binding motif protein 15/15B (RBM15/15B).[12] The demethylation of m^{6}A can be accomplished by the presence of alky-

lation repair homolog protein 5 (ALKBH5), as well as fat mass and obesity-associated protein (FTO), which are recognized as "m6A erasers." In addition, m6A modification is recognized by "m6A readers" such as YTH *N*6-methyladenosine RNA binding proteins (YTHDF), comprising cytoplasmic protein YTHDF1, YTHDF2, and YTHDF3 and nuclear protein YTHDC1.[7] METTL3 is the primary component of the methyltransferase complex and has been implicated in various biological processes, including the self-renewal and differentiation of stem cells,[13,14] cardiac homeostasis,[15] cerebellar development,[16] neurogenesis,[17] and cancers.[18] In particular, loss of METTL3 function in mice leads to embryonic lethality because of immature vascularization.[13] Furthermore, endothelial-specific deletion of METTL3 inhibits Notch signaling, thereby affecting the functions of hematopoietic stem and progenitor cells.[19] Additionally, the ablation of METTL3 leads to a notable suppression of both corneal and retinal neovascularization, attributed to its impact on low-density lipoprotein receptor–related protein 6 (LRP6) and disheveled (DVL1).[20] However, the precise mechanism underlying METTL3-mediated m6A modification in regulating retinal angiogenesis remains unclear.

Here we determined the role of m6A modification and METTL3 in the context of oxygen-induced retinopathy (OIR) mice. Our findings revealed a noticeable increase in m6A modification and METTL3 levels in both the retina and RECs of the OIR mouse model, as well as in hypoxic human retinal microvascular endothelial cells (HRMECs). Furthermore, we found that knockdown of METTL3 significantly inhibited HRMEC tube formation and migration under both hypoxic and normoxic conditions. This effect was associated with decreased m6A levels in matrix metallopeptidase 2 (*MMP2*) and TEK receptor tyrosine kinase (*TIE2*) transcripts, leading to a reduction in their corresponding protein expressions. These results suggest that the METTL3-m6A-MMP2/TIE2 signaling axis plays a critical role in retinal angiogenesis, and that METTL3 may represent a promising target for suppressing retinal neovascularization in clinical settings.

MATERIAL AND METHODS

Mouse Model of OIR

As previously described,[21] mouse pups, along with their nursing mothers, were exposed to $75 \pm 2\%$ O_2 in an incubator between postnatal day (P) 7 and P12 and were then returned to room air. An oxygen controller (Biospherix Ltd, Lacona, NY, USA) was used to check oxygen levels continually. Pups of the same age reared in a normal environment served as the control groups. At P17, retinas and RECs were harvested for subsequent analyses.

All the animal experiments were conducted in compliance with the recommendations of the Association for Research in Vision and Ophthalmology, and approval of the Wenzhou Medical University Animal Care and Use Committee.

Mouse Retinal Endothelial Cell Isolation

RECs were procured from both the OIR and control mice following a previously established protocol.[22] Eyeballs from 17-day-old mouse pups were enucleated, and under microscopic guidance, the corneas were removed. Both the scle-

ras and choroids were meticulously separated from the retinas. These retinas were aseptically dissected, finely minced, and digested using 1 mg/mL type I collagenase (Worthington Biochemical, Lakewood, NJ, USA) at 37°C for 30 minutes. The samples were then spun in a centrifuge, and the resulting pellet was resuspended in sterile PBS containing 1% BSA. This suspension was exposed to magnetic beads (sheep anti-rat; Invitrogen, Carlsbad, CA, USA) that had been precoated with rat anti-mouse CD31 antibody (BD Biosciences, San Diego, CA, USA). After rotation-based incubation and thorough washing to ensure affinity binding, RECs attached to the beads were harvested for m6A dot blot assay.

Immunofluorescence Staining

For immunofluorescence staining, eyeballs from the OIR and control mice at P17 were used. After enucleation, they were encased in an optical cutting temperature compound (OCT; Thermo Fisher Scientific, Waltham, MA, USA) and snap-frozen in liquid nitrogen. The frozen samples were sectioned to a thickness of 10 μm. They were subsequently stabilized in 4% paraformaldehyde for an hour. Following three PBS washes, the samples were permeabilized and blocked with 0.5% tritonX-100 and 5% goat serum for an hour at room temperature. Primary antibody incubation involved anti-METTL3 (1:100; Cell Signaling Technology, Beverly, MA, USA) and anti-GS-ib4 (1:100, Alexa Fluor 594 Conjugate; Thermo Fisher Scientific) and was conducted overnight at 4°C. The samples were then exposed to a fluorescent secondary antibody (Thermo Fisher Scientific) in a 1:400 dilution, incubated at room temperature for an hour, and protected from light. After three subsequent PBS washes, the sections were treated with an anti-fluorescence quenching agent imbued with 4'-6-diamidino-2-phenylindole (DAPI, Invitrogen) and imaged via confocal microscopy (LSM 880; Zeiss, Jena, Germany).

Cells and Treatments

HRMECs (Angio-Protemie, Boston, MA, USA) were cultured in endothelial cell medium (ECM; ScienCell, San Diego, CA, USA) supplemented with 2.5% fetal bovine serum and endothelial cell growth supplement and maintained at 37°C in a humidified 5% CO_2 incubator. All experiments used HRMECs up to the eighth passage. For hypoxia treatments, HRMECs were placed in a sealed chamber maintaining an oxygen concentration of 1%, with levels continuously monitored using an oxygen controller (Biospherix Ltd).

Small Interfering RNA (siRNA) Transfection

Upon reaching 50% confluency, HRMECs underwent transfection using specific siRNA sequences, combined with Lipofectamine RNAiMAX (Invitrogen), in accordance with the manufacturer's guidelines. At six hours after transfection, the culture medium was refreshed. The targeted sequences for the siRNA experiments were as follows: siMETTL3-1: 5′-GCA AGA ATT CTG TGA CTA T-3′; siMETTL3-2: 5′-GCT GCA CTT CAG ACG AAT T-3′; siMMP2: 5′-GCA CCC AUU UAC ACC UAC A-3′; siTIE2: 5′-CCU UCC UAC CAG CUA CUU U-3′; Negative control (NC) siRNA: 5′-U UC UCC GAA CGU GUC ACG U-3′. The efficacy of gene knockdown was subsequently validated through Western blot analysis.

Transwell Migration Assay

HRMECs, after transfection with siRNA, were collected post-trypsinization and subsequently resuspended in ECM. A cell suspension of 2×10^4 cells/100 μL was added to the upper chambers of transwell plates (8 μm pore size; Corning Inc., Corning, NY, USA). After a 24-hour incubation at 37°C, cells were fixed in 4% paraformaldehyde for 30 minutes at room temperature. Subsequently, cells were stained with crystal violet. Any cells that had not migrated and remained on the upper surface of the membrane were gently wiped away. Migrated cells were photographed using a phase contrast microscope (magnification $\times$ 100; Imager Z1; Zeiss). Migrated cells were quantified from five random fields, and the average number of cells traversing the filter was determined. The assay was performed in triplicate.

Tube Formation Assay

HRMECs (2×10^4) transfected with either NC or target gene siRNA were seeded onto a 96-well plate pre-coated with 60 μL of polymerized Matrigel basement membrane substrate (BD Biosciences). After an eight-hour incubation at 37°C in a 5% CO_2 environment, tube formation was visualized, and images were captured using a microscope outfitted with a camera (Imager Z1, Zeiss). The cumulative length and number of nodes of the formed tubes were analyzed in three arbitrary microscopic fields using the ImageJ software (National Institutes of Health, Bethesda, MD, USA). This experiment was consistently executed in triplicate.

Cell Proliferation Assay

MTS Assay. HRMECs were seeded with a density of 2×10^3 per well in 96-well plates. After 48 hours of siRNA transfection, the cells were incubated with 85 μL F12 culture medium and added 15 μL MTS assay solution (Promega Corp., Madison, WI, USA) per well for two hours at 37°C in a 5% CO_2 incubator. Absorbance was subsequently measured at 490 nm using an M5 plate reader (Molecular Devices, San Jose, CA, USA).

5-Ethynyl-2′-Deoxyuridine (EdU) Assay. EdU assay was performed using the Click-iT EdU imaging kit (Thermo Fisher Scientific). After siRNA transfection, HRMECs were incubated with 10 μM EdU for two hours and then fixed and permeabilized. EdU was detected by incubating with Click-iT reaction mixture for 30 minutes, shielded from light. Cell nuclei were counterstained with DAPI. Visualization and imaging of the labeled cells were performed using a confocal microscope (LSM 710; Zeiss).

Flow Cytometry Analysis. Forty-eight hours after siRNA transfection, HRMECs were collected, and their DNA was stained using propidium iodide (Thermo Fisher Scientific) following the provided protocol. The distribution of cells across different phases of the cell cycle was subsequently analyzed using flow cytometry (FACS caliber; BD Biosciences).

RNA m⁶A Dot Blot Assay

RNA was isolated from cells (RECs or HRMECs) and retinas (from the OIR or control mice). To eliminate DNA contamination, the isolated RNA was treated with DNase I (Roche Diagnostics, Mannheim, Germany) and subsequently denatured at 95°C for five minutes. A consistent volume of 2 μL RNA was then applied to a pre-prepared nylon membrane (Thermo Fisher Scientific). After cross-linking the membrane using ultraviolet radiation for one minute, it was blocked with 5% non-fat milk in PBS infused with 0.1% tween. The membrane was then incubated with an anti-m⁶A antibody (1:1000; Synaptic Systems, Goettingen, Germany) overnight at 4°C. After this, the membrane was exposed to a horseradish peroxidase–conjugated secondary antibody (1:3000; CST) for one hour and subsequently washed thrice with PBS infused with 0.1% tween. The chemiluminescence signals were visualized using electrochemiluminescence reagents (Thermo Fisher Scientific), and dot densitometry was assessed using ImageJ software (NIH).

Methylated RNA Immunoprecipitation (MeRIP)-qPCR

RNA isolated from the NC or METTL3-siRNA transfected HRMECs was treated with DNase I (Roche Diagnostics). An equal amount of RNA was incubated with beads conjugated either to an anti-m⁶A antibody or to a rabbit anti-IgG antibody (Millipore, Seattle, WA, USA) in MeRIP reaction mixture (20 mM Tris pH7.5, 140 mM NaCl, 1% NP-40, and 2 mM EDTA) with rotation for three hours at 4°C. The samples were washed twice in elution buffer containing N^6-methyladenosine with rotation for one hour at 4°C. The RNA was isolated using the RNeasy mini kit (Qiagen, Valencia, CA, USA), which was eluted by adding 14 μL RNase-free water. The purified RNA was then subjected to analysis by qPCR employing the One-Step RT-PCR Reagent (Bio-Rad Life Science, Hercules, CA, USA). The percentage of m⁶A relative to the input in the IP sample was quantified using the $2^{(-\Delta Ct \text{ [normalized IP]})}$ method.

Quantitative Reverse Transcription PCR

TRIzol reagent (Invitrogen) was used to isolate total RNA from retinas or cells in accordance with the manufacturer's recommendations. From this, 1μg of total RNA was subjected to reverse transcription into cDNA using the reverse transcription system (Promega) and random primers. Subsequent quantitative PCR was performed using the Power SYBR green PCR master mix (Thermo Fisher Scientific). The relative gene expression levels were assessed using the $2^{-\Delta\Delta CT}$ method. *ACTB* expression level was used as reference genes for normalization. Primer sequences used in the experiments are provided in the supplementary data.

Western Blot

HRMECs or retinas were lysed in ice-cold RIPA lysis buffer (Beyotime Biotechnology Inc., Shanghai, China) containing a protease inhibitor cocktail (Merck, Darmstadt, Germany). The resulting lysates were separated through SDS-PAGE and subsequently transferred onto nitrocellulose blotting membranes (0.2 μm; GE Healthcare Life Sciences, Uppsala, Sweden). These membranes were incubated overnight at 4°C with specific primary antibodies: METTL3 (1:1000; Abcam), METTL14 (1:1000; Invitrogen), WTAP (1:1000; CST), FTO (1:1000; Santa Cruz Biotechnology, Inc., Dallas, TX, USA), ALKBH5 (1:1000; Novus Biologicals, Littleton, CO, USA), MMP2 (1:1000; CST), TIE2 (1:1000; CST), HIF-1α (1:1000; Abcam), and β-ACTIN (1:1000; Santa Cruz Biotechnology). After primary antibody binding, membranes were exposed

to fluorescence-conjugated secondary antibody (goat anti-rabbit/mouse IRDye; LI-COR Biosciences, Lincoln, NE, USA) that had been diluted in the blocking buffer. Bands reactive to the antibodies were revealed with the infrared imaging capabilities of the Odyssey system (LI-COR Biosciences), and their relative densities were quantified using ImageJ software (NIH).

Statistical Analysis

Data from three or more independent experiments are reported as mean $\pm$ standard error of mean (SEM). P values were determined using two-tailed Student's t test. A P value < 0.05 was considered to be statistically significant. $*P < 0.05$; $**P < 0.01$; $***P < 0.001$.

RESULTS

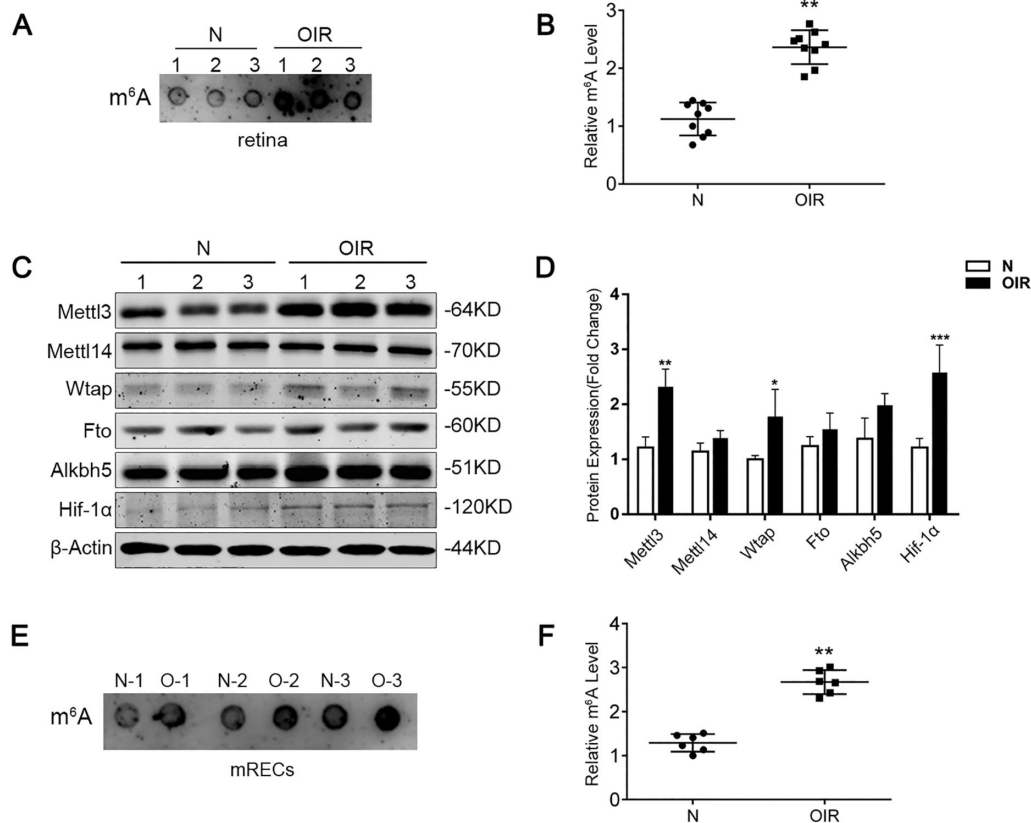### Elevation of m⁶A Modification Levels in the Retina and RECs of the OIR Mouse Model

To determine the role of m⁶A modification in retinal neovascularization, we first quantified the m⁶A modification levels in an OIR mouse model. Using the RNA m⁶A dot blot assay, the retinas of OIR mice displayed approximately a two-fold increase in global m⁶A levels compared to the controls (2.32 ± 0.23 vs 1.22 ± 0.14; Figs. 1A, 1B). Subsequent west-

ern blot analysis of the retinas revealed a pronounced upregulation of METTL3 (2.32 ± 0.25 in OIR retinas vs 1.34 ± 0.15 in control retinas). However, the protein expression of METTL14 remained consistent. Likewise, the protein levels of the demethylases ALKBH5 and FTO did not exhibit any discernible alteration (Figs. 1C, 1D).

Considering the instrumental role of vascular endothelial cells in angiogenesis, we gauged m⁶A modification levels in retinal vascular endothelial cells extracted from the OIR mice. Our findings highlighted an approximate two-fold surge in m⁶A modification in the RECs of the OIR model relative to the controls (Figs. 1E, 1F). Immunofluorescence staining provided insight into the localization and expression of METTL3 in these cells. Notably, METTL3 was predominantly localized in the nuclei of retinal vascular endothelial cells. Furthermore, its expression was conspicuously amplified in the neovascular endothelial cells derived from OIR retinas in comparison to the control mice (Supplementary Fig. S1).

Hypoxia Enhances m⁶A Modification Levels in HRMECs

Hypoxic stress has been identified as a major driver in the development of retinal neovascularization. To explore the implications of RNA m⁶A modification in dictating

FIGURE 1. The profile of m⁶A modification in the retinas and retinal endothelial cells of OIR mice. (**A**) Dot blot analysis showcasing representative images of m⁶A modification levels in the retinas from both the OIR and control groups. (**B**) Quantitative assessment of m⁶A modification levels from the dot blot analysis (n = 9/group). (**C**) Western blot analysis detected the protein expression levels of Mettl3, Mettl14, Wtap, Fto, and Alkbh5 in the retinas of the OIR and control mice. (**D**) Quantification of respective protein expression levels (n = 9/group). (**E**) Dot blot representation and (**F**) subsequent quantification of RNA m⁶A levels in retinal endothelial cells from the OIR and control mice (n = 6/group). N, normal mouse; OIR, oxygen-induced retinopathy mouse; mRECs, mouse retinal endothelial cells.
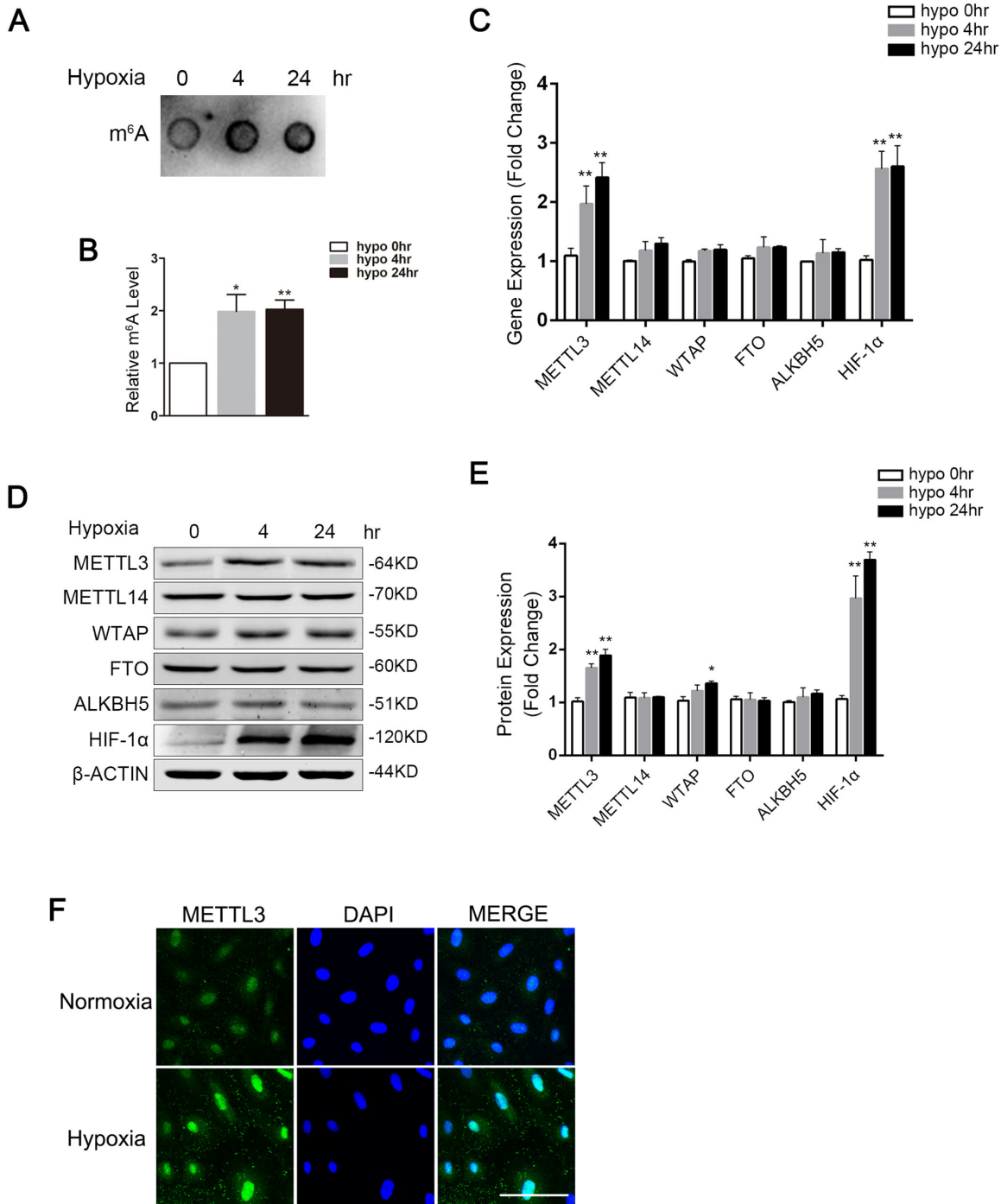
Figure 2. RNA m^{6}A modification levels increase in HRMECs under hypoxic conditions. (**A**) A representative dot blot image depicting RNA m^{6}A modifications in HRMECs after four and 24 hours' exposure to 1% O$_2$, juxtaposed with normoxic conditions (21% O$_2$). (**B**) Statistical analysis of m^{6}A modification levels from dot blot results (n = 3/group). (**C**) RT-qPCR results displaying expression patterns of m^{6}A methyltransferases (*METTL3, METTL14, WTAP*) and demethylases (*FTO, ALKBH5*) in HRMECs subjected to hypoxic and normoxic atmospheres (n = 3/group). (**D**) Western blot representation detailing protein levels of METTL3, METTL14, WTAP, FTO, ALKBH5, and HIF-1α in HRMECs under 21% O$_2$ or 1% O$_2$ exposure. (**E**) Relative protein expression quantification (n = 3/group). (**F**) Immunofluorescence reveals nuclear localization of METTL3 (*green*) in retinal endothelial cells, with enhanced fluorescence intensity under hypoxic conditions compared to normoxic states. DAPI (*blue*) marks cell nuclei. *Scale bar:* 100 µm.

endothelial responses under hypoxic challenges, we subjected HRMECs to 1% O$_2$ and subsequently performed dot blot assays. The analyses revealed a noteworthy augmentation of global m^{6}A modification levels, nearly doubling in the hypoxic group relative to the normoxic controls (Figs. 2A, 2B).

In our quest to decipher the underlying mechanisms for this m^{6}A elevation, we scrutinized the expression patterns of
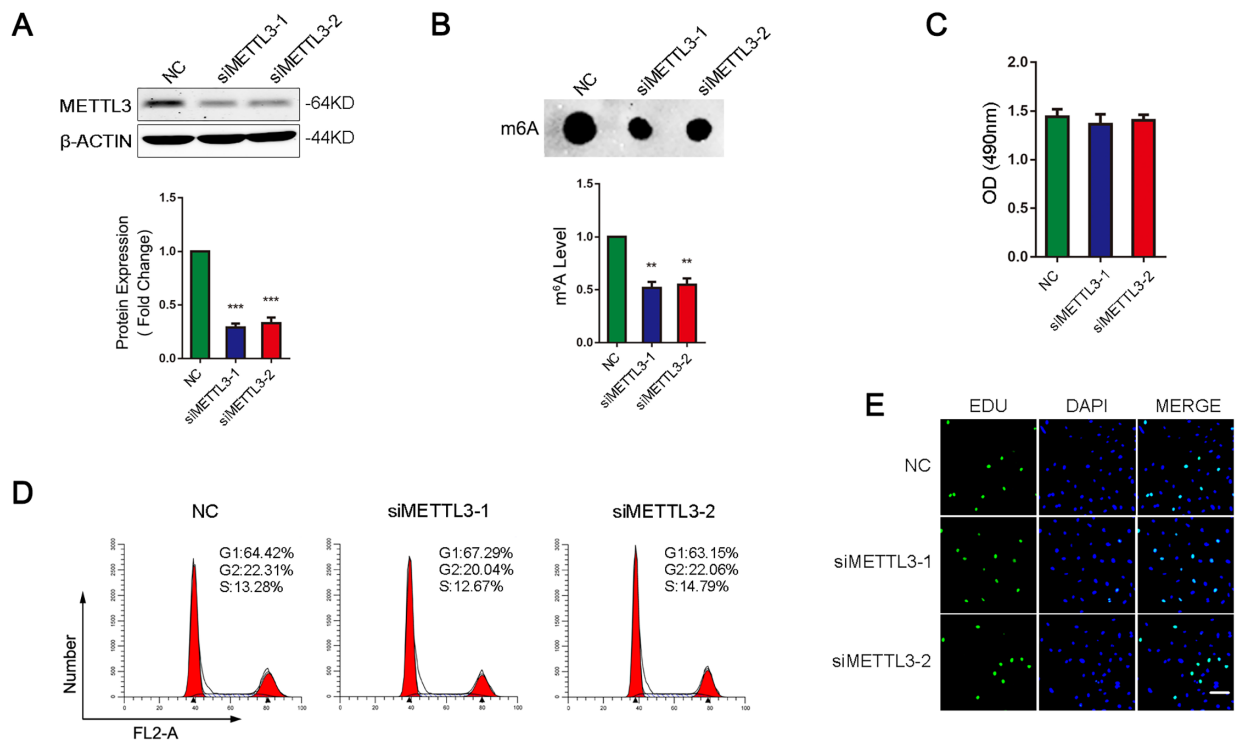
FIGURE 3. Impacts of METTL3 suppression on HRMEC proliferation. (**A**) Western blot results accompanied by quantitative data, displaying METTL3 expression in HRMECs post-transfection with METTL3-specific siRNAs (n = 3/group). (**B**) Depictive dot blot images and subsequent quantitative evaluation of RNA m^{6}A modification levels in HRMECs after METTL3 siRNA transfection compared to control cells (n = 3/group). (**C**) Proliferative capabilities of METTL3 siRNA and NC siRNA-treated cells assessed via MTS assay (n = 3/group). (**D**) Cell cycle distribution of METTL3 siRNA or NC transfected HRMECs analyzed through flow cytometry. (**E**) Fluorescence imagery of EDU staining in HRMECs after METTL3 or NC siRNA treatments. NC, Negative Control. *Scale bar:* 200 μm.

relevant methyltransferases (METTL3, METTL14, and WTAP) and demethylases (FTO and ALKBH5). RT-qPCR data indicated a pronounced surge in *METTL3* mRNA expression in HRMECs under 1% O_2 exposure (1.87 ± 0.27 after 4 hours and 2.22 ± 0.30 after 24 hours) compared to its normoxic counterparts. However, the mRNA expression profiles of *ALKBH5* and *FTO,* remained consistent (Fig. 2C). Parallel observations were made at the protein level: METTL3 concentrations were elevated after four hours (1.45 ± 0.14) and 24 hours (1.72 ± 0.22) of hypoxia exposure, whereas ALKBH5 and FTO protein levels remained static (Figs. 2D, 2E).

To map the intracellular distribution of METTL3, we employed immunofluorescence staining techniques. These assays confirmed that METTL3 predominantly resides in the nucleus of endothelial cells and highlighted its increased expression in cells exposed to hypoxia (Fig. 2F).

Downregulation of METTL3 Impedes Migration and Tube Formation in HRMECs

To elucidate the role of METTL3 in modulating hypoxia-induced angiogenesis, we assessed the angiogenic effects post METTL3 knockdown (KD) in HRMECs. For KD, we used two distinct siRNAs targeting different regions of the *METTL3* transcript. Western blot results corroborated that both siRNAs effectively curtailed METTL3 protein expression, demonstrating a reduction of over 70% (Fig. 3A). Subsequently, the influence of METTL3 KD on m^{6}A modi-

fication levels in total RNAs was examined. A dot blot assay revealed a reduction of m^{6}A levels by approximately 45% upon METTL3 KD (0.52 ± 0.03 for METTL3-1 KD and 0.55 ± 0.04 for METTL3-2 KD relative to the control; Fig. 3B).

Shifting our focus to the biological implications of METTL3 KD on HRMECs, comprehensive tests including the MTS assay, EDU assay, and cell cycle analysis collectively indicated no discernible effects of METTL3 KD on retinal endothelial cell proliferation (Figs. 3C–E).

Conversely, evaluations using a Matrigel-based tube formation assay revealed that METTL3 KD markedly curbed endothelial tube formation under normoxic conditions (node count: 30.33 ± 1.76 for the NC group, 18.67 ± 0.88 for the siMETTL3-1 group, and 19.33 ± 0.33 for the siMETTL3-2 group; Figs. 4A, 4B). Recognizing the pivotal role of cell migration during angiogenesis, we employed an in vitro transwell assay to assess endothelial migration. The data pinpointed a decline of nearly 45% in migrated cell numbers for the METTL3 KD cohorts (270 ± 1.33 in the control, 151 ± 2.60 in the siMETTL3-1, and 147.3 ± 8.41 in the siMETTL3-2 groups; Figs. 4C, 4D). Under hypoxic conditions, the METTL3 KD groups, when subjected to 1% O_2, demonstrated a suppressed augmentation in endothelial tube formation (node count: 37 ± 1.73 for the NC group, 24.67 ± 0.33 for the siMETTL3-1 group, and 25.67 ± 0.33 for the siMETTL3-2 group; Figs. 4E, 4F). Correspondingly, the proclivity for endothelial migration under hypoxic conditions was diminished by 45%, as evidenced by the comparison with the control (407 ± 13.05 for the NC group,
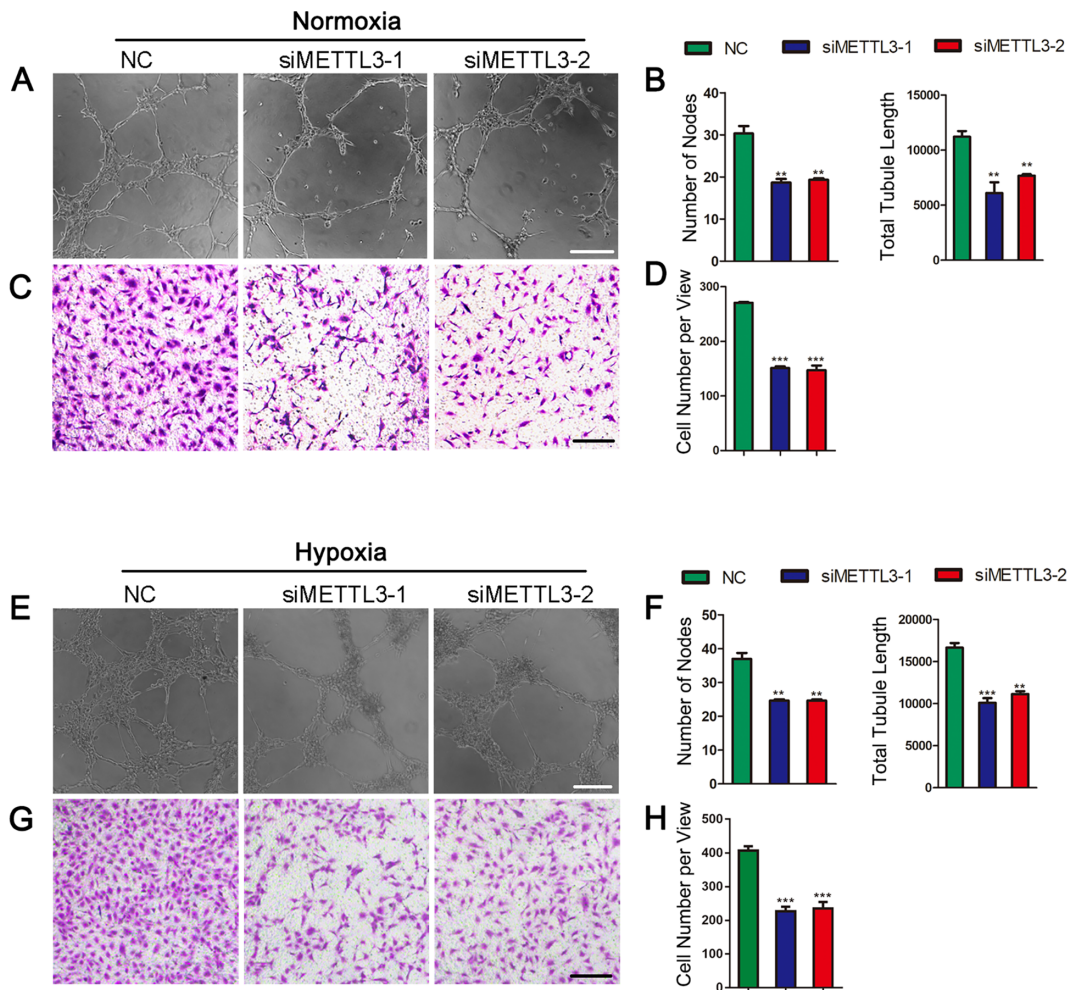
FIGURE 4. Effects of METTL3 inhibition on angiogenic responses in HRMECs. (**A**) Matrigel-based tube formation assay under normoxic conditions, revealing compromised tube formation in METTL3 siRNA-treated HRMECs. (**B**) Quantitative assessment of tube node count and cumulative tube length derived from the Matrigel-based angiogenesis assay (n = 3/group). (**C**) Visual representation of a transwell assay with METTL3 siRNA or NC treated HRMECs in a normoxic environment. (**D**) Quantitative analysis illustrating the number of migratory cells determined through transwell assays (n = 3/group). (**E, F**) Representative imagery and statistical outcomes from Matrigel-based angiogenesis tests involving METTL3 siRNA or NC treated HRMECs under hypoxic conditions (n = 3/group). (**G, H**) Pictorial and quantitative summaries of transwell experiments conducted on METTL3 siRNA or NC treated HRMECs during hypoxia (n = 3/group). NC, negative control. *Scale bar*: 200 µm.

227 ± 13.32 for the siMETTL3-1 group, and 235 ± 19.73 for the siMETTL3-2 group; Figs. 4G, 4H).

METTL3 Modulates m⁶A Modification of Angiogenesis-Associated Transcripts

To decipher the underlying mechanisms by which METTL3 augments retinal endothelial tube formation and migration, we used bioinformatic analyses to identify potential METTL3 downstream targets implicated in m⁶A modification in HRMECs. This revealed a subset of angiogenesis-associated genes that exhibited significant m⁶A modification. Among these, the transcripts of *MMP2*, *TIE2*, *CDC42*, and *PTEN* were notably enriched (Fig. 5A). Using a dedicated web-based tool (http://www.cuilab.cn/scramp/), we predicted m⁶A modification sites within these transcripts. We discerned multiple m⁶A modification sites predominantly localized in the 3′ untranslated regions (UTRs) of these tran-

scripts (Supplementary Fig. S2). Subsequent validation using MeRIP-qPCR confirmed the METTL3-mediated methylation of these identified transcripts. Notably, both *MMP2* and *TIE2*, which serve as pivotal regulators of endothelial migration and angiogenesis, were methylated by METTL3. After METTL3 knockdown, there was a marked reduction in m⁶A modification at these sites (*MMP2* transcript m⁶A content: 42.86% ± 4.19% in the siMETTL3-1 group and 58.24% ± 3.88% in the siMETTL3-2 group; *TIE2*: 51.11% ± 1.86% in the siMETTL3-1 group and 58.32% ± 2.52% in the siMETTL3-2 group when juxtaposed with the NC group; Fig. 5B). Nonetheless, METTL3 silencing elicited negligible effects on the mRNA expression levels of *MMP2* and *TIE2* (Fig. 5C). However, a METTL3 knockdown led to a prominent reduction in the protein levels of MMP2 and TIE2 by 40% and 45% under normoxic and hypoxic conditions, respectively (Figs. 5D, 5E). To further determine whether METTL3 functions upstream of MMP2 and TIE2, we analyzed the protein expression of METTL3 after the silencing of MMP2 and
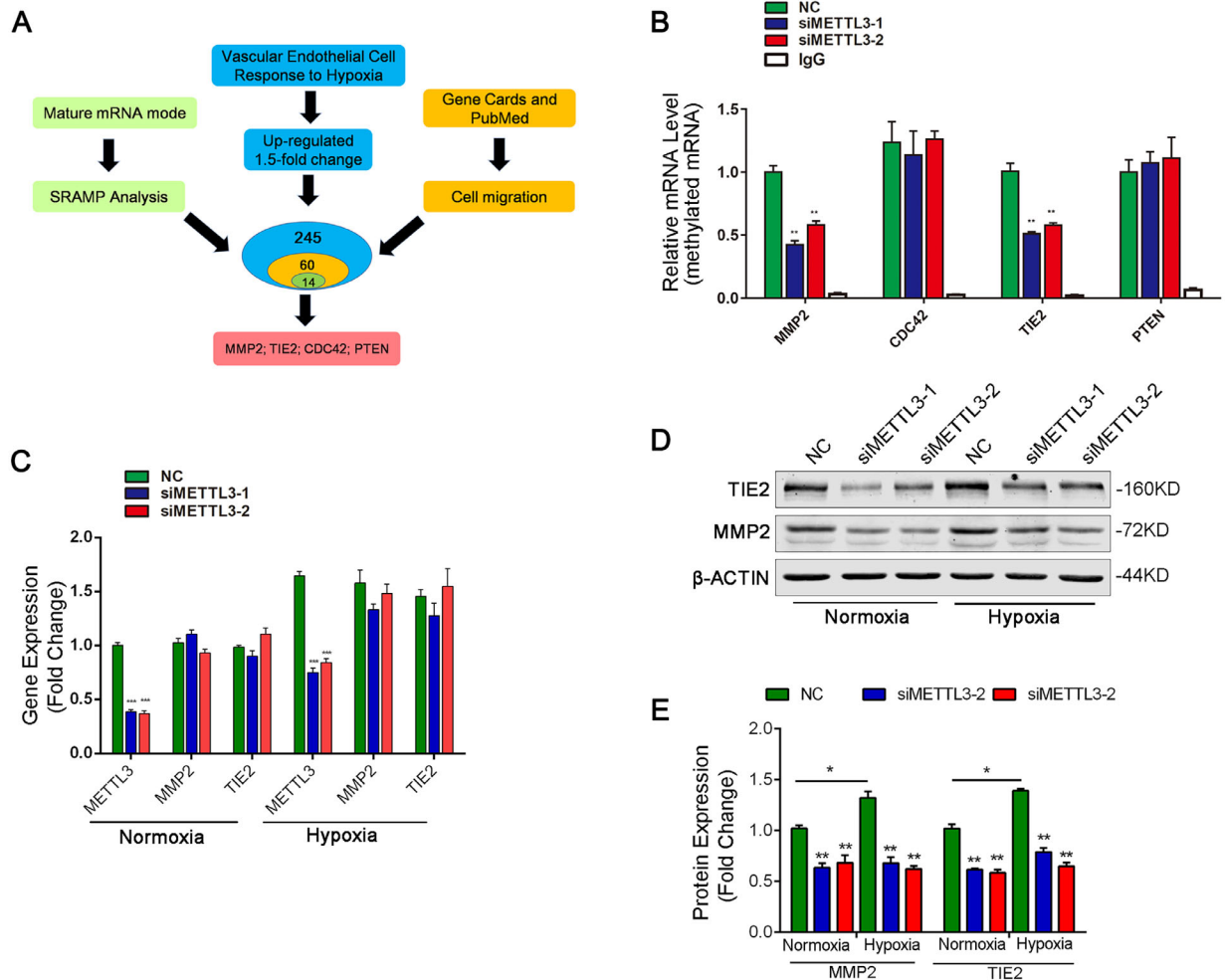
FIGURE 5. METTL3 regulates m^{6}A modification in *MMP2* and *TIE2* transcripts. (**A**) Schematic representation outlining the strategy for identifying potential targets influenced by METTL3. (**B**) MeRIP-qPCR assay delineating the relative m^{6}A enrichment in *MMP2, CDC42, TIE2,* and *PTEN* transcripts in METTL3 siRNA-treated HRMECs relative to the negative control group (n = 3/group). (**C**) RT-qPCR quantification of *MMP2* and *TIE2* mRNA expression in HRMECs post-transfection with METTL3 or NC siRNA (n = 3/group). (**D**) Protein expression levels of MMP2 and TIE2 in HRMECs post METTL3 siRNA or NC transfection, assessed under both normoxic (21% O$_2$) and hypoxic (1% O$_2$) conditions using Western blot. (**E**) Densitometric analysis of the protein bands from the Western blot (n = 3/group).

TIE2. Western blot analyses revealed consistent levels of METTL3 protein in HRMECs in which MMP2 and TIE2 had been silenced. Taken in conjunction with prior findings, this strongly suggests that METTL3 serves as an upstream modulator of both MMP2 and TIE2 (Supplementary Fig. S3).

## Attenuation of MMP2 or TIE2 Dampens Angiogenic Capacities of HRMECs

To determine whether the influence of METTL3 on HRMEC angiogenic behavior is mediated by its modulation of MMP2 and TIE2 protein expression, we assessed the individual impact of silencing MMP2 and TIE2 on HRMEC migration and tube formation, both under normoxic and hypoxic conditions. Using a Matrigel-based angiogenesis assay, our data illustrated a marked reduction in endothelial tube formation by 30% in siMMP2-transfected HRMECs and by 35% in siTIE2-transfected cells (node count: 40.33 ± 1.76 in the NC group, 29 ± 0.57 in the siMMP2 group, and 27.33 ± 0.88 in the siTIE2 group; see Figs. 6A and 6B). Addi-

tionally, migration assays depicted a decline in migratory activity by 45% for siMMP2-transfected cells and by 40% for siTIE2-transfected cells when compared to the NC group (cell counts: 234.7 ± 8.11 in the NC group, 137 ± 4.93 in the siMMP2 group, and 158.7 ± 8.41 in the siTIE2 group; refer to Figs. 6C and 6D). Moreover, under hypoxic conditions, silencing either MMP2 or TIE2 consistently impeded the migratory and tube formation capacities of the endothelial cells (node count: 44.33 ± 1.52 in the NC group, 23.33 ± 1.20 in the siMMP2 group, and 28.33 ± 1.45 in the siTIE2 group; transwell assay: 313.3 ± 8.81 in the NC group, 174.3 ± 8 in the siMMP2 group, and 187 ± 12.77 in the siTIE2 group; see Figs. 6E–H). In summary, analogous to the effects seen with METTL3 silencing, the attenuation of MMP2 or TIE2 similarly curbed the angiogenic potential of HRMECs in both normoxic and hypoxic environments.

DISCUSSION

Retinal angiogenesis, a multifaceted process, is indispensable for the proper growth and maturation of the retina.
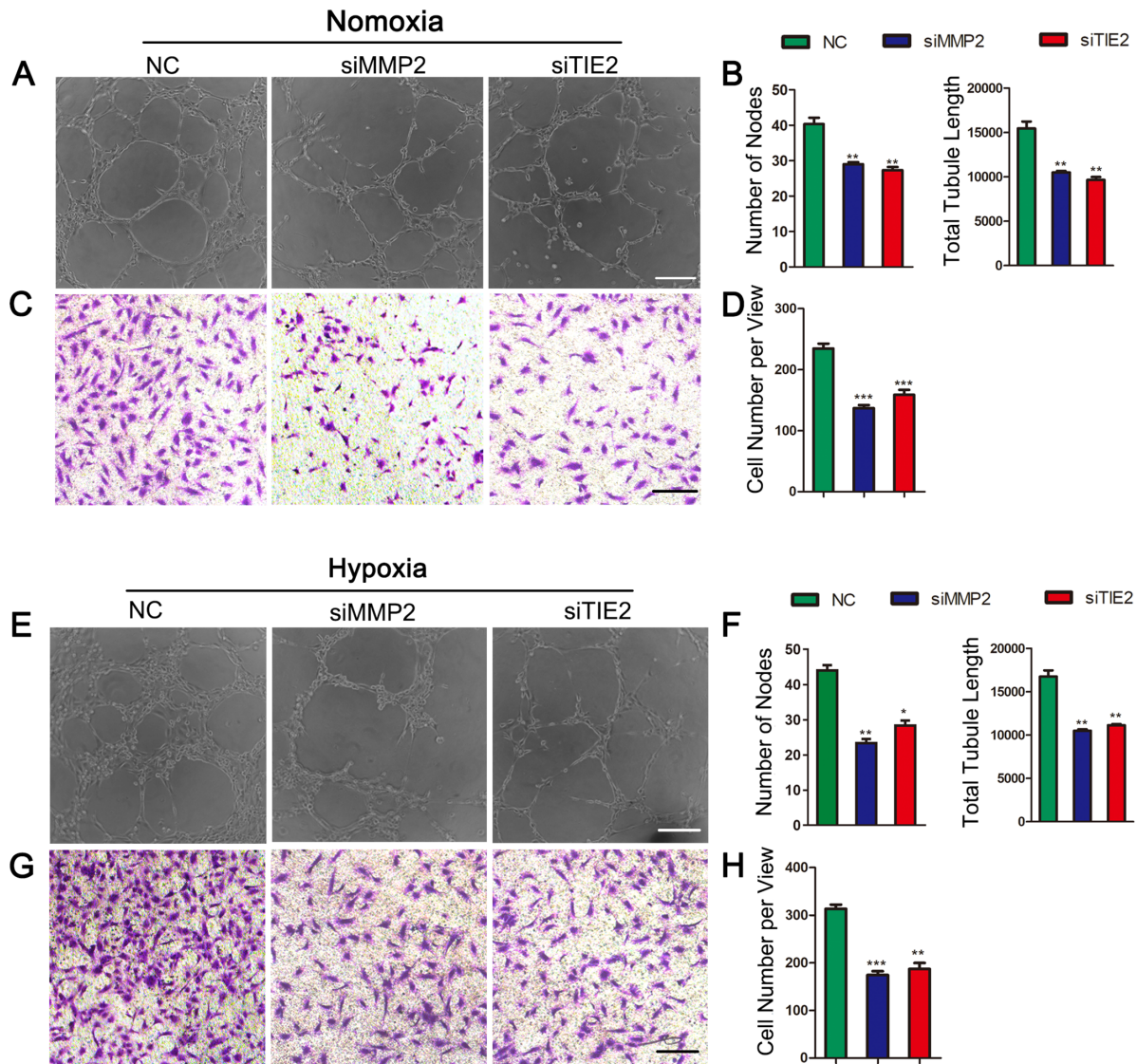
FIGURE 6. Consequences of MMP2 or TIE2 inhibition on HRMEC angiogenic activities. (**A**) In vitro Matrigel-based angiogenesis assay illustrating the tube formation capabilities of MMP2, TIE2, and NC siRNA-transfected HRMECs under normoxic conditions. (**B**) Quantitative data reflecting the number of nodes and cumulative tube length from the in vitro Matrigel-based angiogenesis assay (n = 3/group). (**C**) Representative imagery from the transwell assay assessing endothelial migration potential. (**D**) Quantitative assessment of migratory cells derived from transwell assays (n = 3/group). (**E**) Under hypoxic conditions, the in vitro Matrigel-based angiogenesis assay highlights the tube formation proficiency of MMP2, TIE2, or NC siRNA-transfected HRMECs. (**F**) Quantitative evaluation of the in vitro Matrigel assays under hypoxia (n = 3/group). (**G**) In the context of hypoxia, the transwell assay unveils the migratory capabilities of HRMECs post-transfection with MMP2, TIE2, or NC siRNA. (**H**) Quantitative data detailing the number of migrating cells from the hypoxic transwell assays (n = 3/group). *Scale bar*: 200 μm.

N^6-methyladenosine stands as the predominant RNA modification in eukaryotic cells. However, only recently have the specific roles and underlying mechanisms of m⁶A in retinal angiogenesis started to emerge. In our recent investigation, we observed a pronounced augmentation in m⁶A modification levels within the retina and its endothelial cells in an OIR mouse model. Hypoxia acts as a potent stimulus for neovascularization, and congruently, we noted an elevation in m⁶A modification levels in HRMECs post-hypoxic challenge. Corroborating our findings, an escalated m⁶A modification was reported under hypoxic conditions in HEK293T cells, which subsequently led to the post-transcriptional stabilization of certain mRNAs.[23] Contrarily, diminished m⁶A modification levels were documented

in both HeLa and SMMC7721 cells after hypoxia, coinciding with an upregulated expression of the m⁶A demethylase, ALKBH5.[24] This trend was also mirrored in hypoxia-exposed breast cancer cells.[25] Cumulatively, these observations underscore a pivotal yet intricate role m⁶A modification plays under hypoxic conditions, which appears to be governed by tissue or cell-specific dynamics.

The equilibrium of m⁶A modification is delicately maintained by the interplay of m⁶A writers and erasers. In our investigation, METTL3 expression was notably enhanced in the retinas and RECs of OIR mice, as well as in HRMECs subjected to hypoxia. In contrast, the levels of FTO and ALKBH5 remained unchanged. These findings underscore the centrality of METTL3-mediated m⁶A
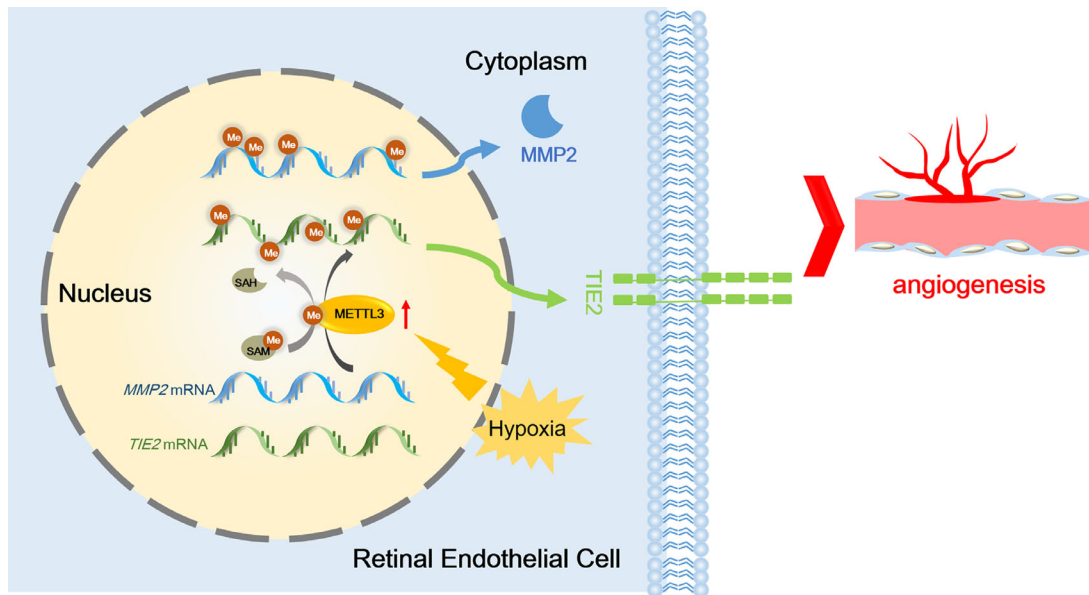
FIGURE 7. Schematic diagram illustrating the METTL3-mediated m[6]A modification of *MMP2* and *TIE2* transcripts and its consequential regulation of angiogenic activities in retinal endothelial cells. SAM, S-adenosylmethionine, methyl donor; SAH, S-adenosylhomocysteine.

modification in hypoxia-driven retinal neovascularization. This is in harmony with Suo et al.,[26] who elucidated that METTL3-mediated m[6]A modification modulates pericyte function during diabetic retinal vascular complications. Moreover, METTL3-mediated m[6]A modification has been linked with the regulation of pathological angiogenesis in diverse tissues, encompassing cerebral arteriovenous malformations,[27,28] and vasculogenic mimicry in hepatocellular carcinoma.[29] Focusing on the core mechanisms of angiogenesis-endothelial cell proliferation and migration, we discerned that silencing METTL3 negligibly impacted endothelial proliferation. However, METTL3 KD notably curtailed migration and tube formation in these cells. Furthermore, the proangiogenic effects induced by hypoxia, especially enhanced migration and tube formation, were attenuated on METTL3 depletion. In alignment with extant literature, METTL3 overexpression has been documented across multiple neoplasms, and its functional inhibition curbed the migratory potential of neoplastic cells,[30–32] underscoring a ubiquitous role of METTL3 in modulating migration across diverse cell populations. In summary, METTL3-dependent m[6]A modification emerges as a pivotal modulator in angiogenesis, directing retinal neovascularization. Thus therapeutic strategies targeting m[6]A modification via METTL3 present a promising avenue for managing neovascularization-associated pathologies.

METTL3 has been recognized for its multifaceted functionality, wherein it modulates target transcripts across various cell types. In our quest to elucidate the modulatory mechanism of METTL3 in angiogenesis, particularly its influence on m[6]A modification within HRMECs, we embarked on both bioinformatic analysis and MeRIP-qPCR assays. Our findings indicated that METTL3 KD precipitated a decline in m[6]A modification levels of *MMP2* and *TIE2* transcripts. Intriguingly, METTL3 KD did not bring about discernible alterations in *MMP2* and *TIE2* mRNA levels in HRMECs; however, a pronounced decrement was observed in their respective protein expressions. Aligning with our observations, Dahal et al.[33] elucidated that silencing METTL3

in melanoma cells attenuated the protein expression of MMP2, which subsequently inhibited migration and invasion. Nonetheless, the intricate mechanics through which METTL3 modulates MMP2 protein expression remain to be comprehensively delineated. In our bioinformatic exploration, we discerned a pronounced m[6]A modification peak proximal to the 3′UTR and the stop codon of MMP2 and TIE2 mRNA. This site is a potential recognition locus for YTHDF1, a known reader of m[6]A modification. Rauch et al. posited that YTHDF1 interaction might potentiate the translational activation of target transcripts, thereby amplifying protein synthesis.[34] Notably, METTL3 can augment the translation of select genes, even independent of its catalytic prowess, by forging interactions with translation initiation complexes.[35] Besides, METTL3 has also been shown to interact with the eukaryotic translation initiation factor 3 subunit h (eIF3h), facilitating mRNA circulation, thereby bolstering gene translation.[36] Against this backdrop, we postulate that METTL3 KD may suppress the translation of *MMP2* and *TIE2* transcripts, a consequence of diminished m[6]A modification levels, culminating in reduced protein expression. The precise methylation sites within *MMP2* and TIE2 transcripts, targeted by METTL3 in HRMECs, warrant a more exhaustive exploration in subsequent research endeavors.

In our study, the effects observed upon knocking down MMP2 and TIE2 mirrored those resulting from METTL3 KD in HRMECs. Notably, increased levels of MMP2 have been reported in patients with proliferative diabetic retinopathy[37] and in animal OIR models.[38] Importantly, MMP2-deficient OIR model mice exhibited diminished retinal neovascularization,[39] underscoring the pivotal role of MMP2 in orchestrating angiogenesis within retinal vascular endothelial cells. TIE2, distinguished as an endothelial-specific receptor tyrosine kinase, is instrumental in both physiological and pathological angiogenic processes.[40,41] Tie2-knockout mice succumb during early embryogenesis, attributed to vascular immaturity and an absence of micro-vessel formation.[42] Moreover, inhibiting TIE2 was shown to thwart pathological

angiogenesis in ischemic retinal conditions.[43] Given the indispensable nature of MMP2 and TIE2 in retinal angiogenesis, a decline in METTL3-mediated m6A modification of these gene transcripts culminated in reduced protein expression levels, subsequently impeding both migration and tube formation in retinal endothelial cells.

Our findings pave the way for an enhanced comprehension of m^{6}A modifications in RECs. As we advance in this research domain, our objectives include the following: (a) A comprehensive identification of m^{6}A targets in RECs using RNA immunoprecipitation followed by deep-sequencing (RIP-seq); (b) Delving deeper into the in vivo functional role and intricate mechanisms of METTL3-mediated m^{6}A modifications in retinal angiogenesis, leveraging the precision of the CRISPR/Cas9 genome editing system; (c) Investigation into the broader clinical implications of m^{6}A modifications in retinal neovascularization disorders, with a particular focus on conditions like neovascular age-related macular degeneration and diabetic retinopathy; (d) Pioneering the conception and synthesis of small molecule inhibitors that target METTL3. This will serve as a linchpin for potential therapeutic applications in clinical settings. We anticipate that strategies targeting METTL3-dependent m^{6}A modification will complement anti-VEGF therapies in the management of angiogenesis-associated pathologies.

Using the mouse OIR model has been foundational in our study—a model that is ubiquitously acknowledged in the research on retinal neovascularization. However, transposing insights from this model to human pathophysiology is not straightforward. It is imperative to note that rodents lack specific anatomical hallmarks present in humans, most prominently the macula. Moreover, there exists a distinctive divergence in vascular pathology; although the human retinopathy of prematurity model witnesses obliteration chiefly in peripheral vessels, the OIR mouse model demonstrates a predilection for central retinal vessel involvement.[44] Apart from these anatomical considerations, potential molecular and cellular differences between rodents and humans may engender disparate therapeutic outcomes. As a result, although our study using the mouse model provides an indispensable foundation, authenticating these findings in higher-order models, such as primates, is paramount to affirm their translational relevance in human therapeutics.

In summary, our study underscores the importance of m^{6}A modification, mediated by METTL3, in regulating hypoxia-driven angiogenesis. Mechanistically, METTL3 KD attenuated the m^{6}A modification of *MMP2* and *TIE2* transcripts in HRMECs, leading to the suppression of their translation and subsequent inhibition of angiogenic behaviors. These findings suggest the METTL3-m^{6}A-MMP2/TIE2 pathway as a novel mechanism in regulating retinal angiogenesis (refer to Fig. 7), highlighting its potential therapeutic role in various retinal neovascularization disorders.

Disclosure: **Y. Lin**, None; **G. Luo**, None; **Q. Liu**, None; **R. Yang**, None; **P. Sol Reinach**, None; **D. Yan**, None

References

1. Penn JS, Madan A, Caldwell RB, et al. Vascular endothelial growth factor in eye disease. *Prog Retin Eye Res* 2008;27:331–371.

2. Lasse Jørgensen C, Kentaro K, Natsuki K, et al. Macular edema in central retinal vein occlusion correlates with aqueous fibrinogen alpha chain. *Invest Ophthalmol Vis Sci* 2023;64(2):23.

3. Campochiaro PA. Ocular neovascularization. *J Mol Med (Berl)* 2013;91(3):311–321.

4. Cooper MP, Keaney JF, Jr. Epigenetic control of angiogenesis via DNA methylation. *Circulation* 2011;123:2916–2918.

5. Fork C, Gu L, Hitzel J, et al. Epigenetic regulation of angiogenesis by JARID1B-induced repression of HOXA5. *Arterioscler Thromb Vasc Biol* 2015;35(7):1645–1652.

6. Zhang Y, Cai S, Jia Y, et al. Decoding noncoding RNAs: role of microRNAs and long noncoding RNAs in ocular neovascularization. *Theranostics* 2017;7:3155–3167.

7. Fu Y, Dominissini D, Rechavi G, He C. Gene expression regulation mediated through reversible m^{6}A RNA methylation. *Nat Rev Genet* 2014;15:293–306.

8. Wang X, Lu Z, Gomez A, et al. N6-methyladenosine-dependent regulation of messenger RNA stability. *Nature* 2014;505(7841):117–120.

9. Mauer J, Luo X, Blanjoie A, et al. Reversible methylation of m^{6}A$_m$ in the 5′ cap controls mRNA stability. *Nature* 2017;541(7637):371–375.

10. Yue Y, Liu J, Cui X, et al. VIRMA mediates preferential m^{6}A mRNA methylation in 3′UTR and near stop codon and associates with alternative polyadenylation. *Cell Discov* 2018;4:10.

11. Wen J, Lv R, Ma H, et al. Zc3h13 regulates nuclear RNA m^{6}A methylation and mouse embryonic stem cell self-renewal. *Mol Cell* 2018;69:1028–1038.e1026.

12. Patil DP, Chen CK, Pickering BF, et al. m^{6}A RNA methylation promotes XIST-mediated transcriptional repression. *Nature* 2016;537(7620):369–373.

13. Geula S, Moshitch-Moshkovitz S, Dominissini D, et al. Stem cells. m6A mRNA methylation facilitates resolution of naive pluripotency toward differentiation. *Science* 2015;347(6225):1002–1006.

14. Batista PJ, Molinie B, Wang J, et al. m^{6}A RNA modification controls cell fate transition in mammalian embryonic stem cells. *Cell Stem Cell* 2014;15:707–719.

15. Dorn LE, Lasman L, Chen J, et al. The N^6-methyladenosine mRNA methylase METTL3 controls cardiac homeostasis and hypertrophy. *Circulation* 2019;139:533–545.

16. Wang CX, Cui GS, Liu X, et al. METTL3-mediated m6A modification is required for cerebellar development. *PLoS Biol* 2018;16(6):e2004880.

17. Chen J, Zhang YC, Huang C, et al. m^{6}A regulates neurogenesis and neuronal development by modulating histone methyltransferase Ezh2. *Genomics Proteomics Bioinformatics* 2019;17:154–168.

18. Chen XY, Zhang J, Zhu JS. The role of m^{6}A RNA methylation in human cancer. *Mol Cancer* 2019;18:103.

19. Lv J, Zhang Y, Gao S, et al. Endothelial-specific m^{6}A modulates mouse hematopoietic stem and progenitor cell development via Notch signaling. *Cell Res* 2018;28:249–252.

20. Yao MD, Jiang Q, Ma Y, et al. Role of METTL3-dependent N^6-methyladenosine mRNA modification in the promotion of angiogenesis. *Mol Ther* 2020;28:2191–2202.

21. Connor KM, Krah NM, Dennison RJ, et al. Quantification of oxygen-induced retinopathy in the mouse: a model of vessel loss, vessel regrowth and pathological angiogenesis. *Nat Protoc* 2009;4:1565–1573.

22. Lin Y, Li L, Liu J, et al. SIRT1 deletion impairs retinal endothelial cell migration through downregulation of VEGF-A/VEGFR-2 and MMP14. *Invest Ophthalmol Vis Sci* 2018;59:5431–5440.

23. Fry NJ, Law BA, Ilkayeva OR, Holley CL, Mansfield KD. N^6-methyladenosine is required for the hypoxic stabilization of specific mRNAs. *RNA* 2017;23:1444–1455.

24. Wang YJ, Yang B, Lai Q, et al. Reprogramming of m6A epitranscriptome is crucial for shaping of transcriptome and proteome in response to hypoxia. *RNA Biol* 2021;18(1):131–143.

25. Zhang C, Samanta D, Lu H, et al. Hypoxia induces the breast cancer stem cell phenotype by HIF-dependent and ALKBH5-mediated m6A-demethylation of NANOG mRNA. *Proc Natl Acad Sci USA* 2016;113(4):E2047–E2056.

26. Suo L, Liu C, Zhang QY, et al. METTL3-mediated N^6-methyladenosine modification governs pericyte dysfunction during diabetes-induced retinal vascular complication. *Theranostics* 2022;12:277–289.

27. Wang LJ, Xue Y, Huo R, et al. N6-methyladenosine methyltransferase METTL3 affects the phenotype of cerebral arteriovenous malformation via modulating Notch signaling pathway. *J Biomed Sci* 2020;27:62.

28. Wang LJ, Xue Y, Li H, et al. Wilms' tumour 1-associating protein inhibits endothelial cell angiogenesis by m6A-dependent epigenetic silencing of desmoplakin in brain arteriovenous malformation. *J Cell Mol Med* 2020;24:4981–4991.

29. Qiao K, Liu Y, Xu Z, et al. RNA m6A methylation promotes the formation of vasculogenic mimicry in hepatocellular carcinoma via Hippo pathway. *Angiogenesis* 2020;24:83–96.

30. Vu LP, Pickering BF, Cheng Y, et al. The N^6-methyladenosine (m6A)-forming enzyme METTL3 controls myeloid differentiation of normal hematopoietic and leukemia cells. *Nat Med* 2017;23(11):1369–1376.

31. Lin S, Liu J, Jiang W, et al. METTL3 promotes the proliferation and mobility of gastric cancer cells. *Open Med (Wars)* 2019;14:25–31.

32. Chen M, Wei L, Law CT, et al. RNA N6-methyladenosine methyltransferase-like 3 promotes liver cancer progression through YTHDF2-dependent posttranscriptional silencing of SOCS2. *Hepatology* 2018;67:2254–2270.

33. Dahal U, Kang L, Gupta M. RNA m6A methyltransferase METTL3 regulates invasiveness of melanoma cells by matrix metallopeptidase 2. *Melanoma Res* 2019;29:382–389.

34. Rauch S, He C, Dickinson BC. Targeted m6A reader proteins to study epitranscriptomic regulation of single RNAs. *J Am Chem Soc* 2018; 140(38):11974–11981.

35. Lin S, Choe J, Du P, Triboulet R, Gregory RI. The m6A methyltransferase METTL3 promotes translation in human cancer cells. *Mol Cell* 2016;62:335–345.

36. Choe J, Lin S, Zhang W, et al. mRNA circularization by METTL3-eIF3h enhances translation and promotes oncogenesis. *Nature* 2018;561(7724):556–560.

37. Noda K, Ishida S, Inoue M, et al. Production and activation of matrix metalloproteinase-2 in proliferative diabetic retinopathy. *Invest Ophthalmol Vis Sci* 2003;44:2163–2170.

38. Majka S, McGuire P, Colombo S, Das A. The balance between proteinases and inhibitors in a murine model of proliferative retinopathy. *Invest Ophthalmol Vis Sci* 2001;42:210–215.

39. Ohno-Matsui K, Uetama T, Yoshida T, et al. Reduced retinal angiogenesis in MMP-2-deficient mice. *Invest Ophthalmol Vis Sci* 2003;44:5370–5375.

40. Sato TN, Qin Y, Kozak CA, Audus KL. Tie-1 and tie-2 define another class of putative receptor tyrosine kinase genes expressed in early embryonic vascular system. *Proc Natl Acad Sci USA* 1993;90:9355–9358.

41. Risau W. Mechanisms of angiogenesis. *Nature* 1997;386(6626):671–674.

42. Sato TN, Tozawa Y, Deutsch U, et al. Distinct roles of the receptor tyrosine kinases Tie-1 and Tie-2 in blood vessel formation. *Nature* 1995;376(6535):70–74.

43. Takagi H, Koyama S, Seike H, et al. Potential role of the angiopoietin/tie2 system in ischemia-induced retinal neovascularization. *Invest Ophthalmol Vis Sci* 2003; 44:393–402.

44. Grossniklaus HE, Kang SJ, Berglin L. Animal models of choroidal and retinal neovascularization. *Prog Retin Eye Res* 2010;29:500–519.